Determination of the point resolution of high-resolution transmission electron microscope using the through-focus technique

Fukushima, Kurio
STEM Corporation

Taniguchi, Yoshifumi
Core Technology & Solutions Business Group, Hitachi High-Tech Corporation

Matsushita, Mitsuhide
EP Business Unit, JEOL Ltd.

Sugiyama, Masaaki
Research Center for Ultra-High Voltage Electron Microscopy, Osaka Univ.

他

https://hdl.handle.net/2324/7238745

出版情報：Micron. 182, pp.103639-, 2024-07. Elsevier
バージョン：

Point resolution of high-resolution transmission electron microscope (HREM) and its measurement methods.

Kurio Fukushima[1)], Yoshifumi Taniguchi[2)], Mitsuhide Matsushita[3)],
Masaaki Sugiyam[4)] and Kenji Kaneko[5)]

1) STEM Corporation, Tokyo, 194-0215, Japan
2) Core Technology & Solutions Business Group, Hitachi High-Tech Corporation, Ibaragi, 312-8504, Japan
3) EP Business Unit, JEOL Ltd., Tokyo, 196-8558, Japan
4) Research Center for Ultra-High Voltage Electron Microscopy, Osaka Univ., Osaka, 567-0047, Japan
5) Dept. Materials, Graduate School of Engineering, Kyushu Univ., Fukuoka, 819-0395, Japan

Abstract

From the viewpoint of evaluating the instrumental performance of high-resolution electron microscopy (HREM), the Scherzer condition was investigated using information transfer theory. As a result, the optimum defocus amount Δf can be expressed based on $(C_s\lambda)^{\frac{1}{2}}$, and the formula $\Delta f = 1.12(C_s\lambda)^{\frac{1}{2}}$ is obtained. Furthermore, a procedure for measuring point resolution using the through-focus technique is developed, and a new method for determining the spherical aberration coefficient using the variance of Δf is introduced in the procedure.

Keyword

High-resolution TEM, Point resolution, Scherzer resolution, Spherical aberration coefficient, Phase contrast, Information transfer theory

1. Introduction

Since the 1st development of the electron microscope by Max Knoll and Ernst Ruska in 1931 [1], transmission electron microscopes (TEMs) have received large attention both academically and industrially. Today, TEMs are the most advanced and used instruments for nanostructural and nanochemical analyses, and their results are always included in the literature with various "nano" forms. Moreover, since their development, TEMs have been developed with substantial and unceasing efforts for imaging at high magnification and resolution, which has been playing an important role in accomplishing atomic scale characterization of materials to identify atoms and molecules.

Scherzer proposed "Scherzer resolution" by the structure size at the first zero of the phase contrast transfer function (PCTF), which is now generally accepted as the definition of point resolution [2]. Although Scherzer resolution, d_{Sch}, can be expressed using the spherical aberration coefficient of the objective lens, C_S, and the wavelength, λ, as Eq. (1);

$$d_{Sch} = 0.66 C_S^{1/4} \lambda^{3/4} \quad (1)$$

there is no standardized method for measuring Scherzer resolution to determine the TEM performance.

Scherzer condition and Scherzer resolution are summarized based on the model proposed by Scherzer [2]. With a weakly phase object, the phase difference, $\chi(\alpha)$, of the scattered electron passing the object lens at an incident angle, α, and defocus, Δf ($\Delta f > 0$ for under-focus), can be expressed by Eq. (2-1) with the parameters defined as s by Eq. (2-2) and τ by Eq. (2-3) [2].

$$\chi(\alpha) = s^2\alpha^4 - \tau s \alpha^2 \quad (2\text{-}1)$$

$$s = \left(\frac{\pi C_S}{2\lambda}\right)^{\frac{1}{2}} \quad (2\text{-}2)$$

$$\tau = \frac{\pi \Delta f}{\lambda s} = \left(\frac{2\pi}{\lambda C_S}\right)^{\frac{1}{2}} \Delta f \quad (2\text{-}3)$$

When the size of the sample is d, the relationship between the spatial frequency, u, denoted by the reciprocal of d, and α would be given by

$$\alpha = \lambda u \quad (3)$$

so that Eq. (1-1) can be rewritten in the form as Eq. (4).

$$\chi(u) = s^2\lambda^4 u^4 - \tau s \lambda^2 u^2 = \frac{\pi}{2} C_s \lambda^3 u^4 - \pi \Delta f \lambda u^2 \quad (4)$$

When C_s and Δf are determined, $\chi(u)$ is given by a quartic function for u, as shown in Fig. 1, and u^2 is then expressed as Eq. (5-2) from (5-1)

$$\frac{d}{du}\chi(u) = 4s^2\lambda^4u^3 - 2\tau s\lambda^2 u = 2us\lambda^2(2s\lambda^2u^2 - \tau) = 0 \quad (5\text{-}1)$$

$$u^2 = \frac{\tau}{2s\lambda^2} \quad (5\text{-}2)$$

the $\chi_{min}(u)$ is thus expressed in Eq. (6);

$$\chi_{min}(u) = s^2\lambda^4\left(\frac{\tau}{2s\lambda^2}\right)^2 - \tau s\lambda^2\frac{\tau}{2s\lambda^2} = \left(\frac{\tau}{2}\right)^2 - \frac{\tau^2}{2} = -\frac{\tau^2}{4} = -\frac{\pi}{2}\left\{\frac{(\Delta f)^2}{C_s\lambda}\right\} \quad (6)$$

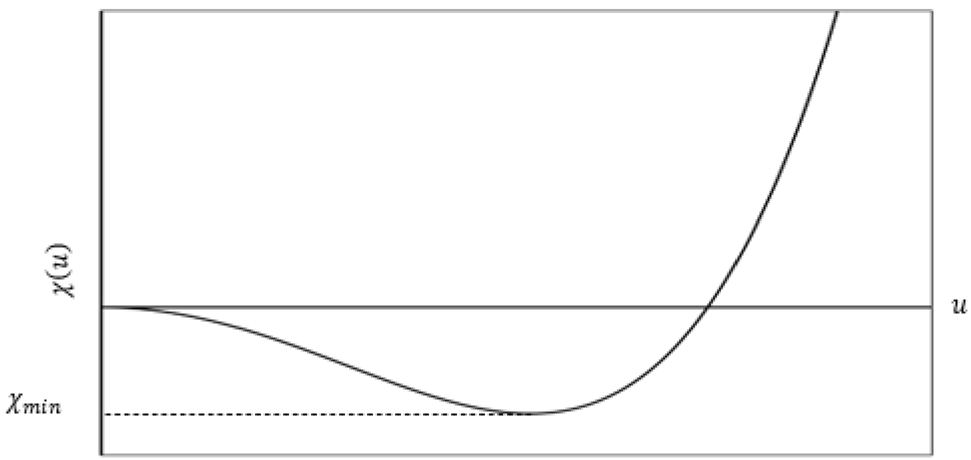

Fig. 1. Example of phase-distortion function, $\chi(u)$.

Since the scattered wave passing through a weakly phased object is delayed in phase by $\pi/2$ with regards to the transmitted wave, a structure with a size corresponding to the spatial frequency u at which the $\pi/2$ phase delay due to $\chi(u)$ having the maximum phase contrast on the image plane. In addition, $\chi(u)$ is a quartic function of u, and it is impossible to satisfy the maximum contrast for all u. Scherzer thus proposed $\tau = 2.5 \sim 3.0$ for the condition (Scherzer condition) where high contrast can be obtained over a wider range of u, and suggested that the optimum defocus value is obtained at $\tau = 3.0$ [2]. For $\tau = 2.5$ and 3.0, $\chi_{\min\,(\tau=2.5)} = -0.5\pi$ and $\chi_{min\,(\tau=3.0)} = -0.7162\pi$. It is then necessary to set the defocus values, Δf_{Sch}, to

$$\Delta f_{Sch\,(\tau=2.5)} = (C_s\lambda)^{\frac{1}{2}} \approx 1[\mathrm{Sch}] \tag{7-1}$$

or

$$\Delta f_{Sch\,(\tau=3.0)} \approx 1.2(C_s\lambda)^{\frac{1}{2}} \approx 1.2[\mathrm{Sch}]. \tag{7-2}$$

Defocus values that satisfy these conditions are called Scherzer defocus. The sine function of $\chi(u)$ is the PCTF. Scherzer resolution, d_{Sch}, is therefore defined as the reciprocal of the u-value where the PCTF curve under Scherzer condition first crosses the horizontal axis (1st Zero), and expressed by Eqs. (8-1) and (8-2) for $\tau = 2.5$ and $\tau = 3.0$, respectively.

$$d_{Sch\,(\tau=2.5)} \approx 0.71(C_s\lambda^3)^{\frac{1}{4}} \approx 0.71[\mathrm{Gl}] \tag{8-1}$$

$$d_{Sch\,(\tau=3.0)} \approx 0.65(C_s\lambda^3)^{\frac{1}{4}} \approx 0.65[\mathrm{Gl}] \tag{8-2}$$

Furthermore, Scherzer focus can be expressed by using Scherzer unit [Sch] based on $(C_s\lambda)^{\frac{1}{2}}$ and the Glaser unit [Gl] based on $(C_s\lambda^3)^{\frac{1}{4}}$ [3].

Even though Scherzer proposed $\tau = 3$ as the optimal defocus value to determine the resolution of HREM [2], O'Keefe pointed out that the optimal defocus value would differ depending on the observing objects [4]. Eisenhandler and Siegel [5] proposed for a single atom, nonetheless;

$$\Delta f_{\mathrm{Sch}(\tau=2.987)} \approx \sqrt{1.42}[\mathrm{Sch}] \tag{9-1}$$

O'Keefe [4] pointed out the weak phase object based on the image simulation as;

$$\Delta f_{\mathrm{Sch}(\tau=3.070)} \approx \sqrt{3/2}\,[\mathrm{Sch}]. \tag{9-2}$$

In addition,

$$\Delta f_{\mathrm{Sch}(\tau=2.507)} \approx 1[\mathrm{Sch}] \tag{9-3}$$

can be proposed as the optimal defocus value, because it provides a flat spatial frequency region with maximum contrast, as shown by the blue line in the PCTF curve in Fig. 2 [6-9].

The optimum defocus values are determined from the viewpoint of maintaining high-contrast over a wider spatial frequency range in the PCTF curve, although there is a raised area in some high-contrast region, arrowed in Fig. 2, as shown by the orange line in Fig. 2. In that case, the typical value for $\chi_{min}(u)$ is $-2/3\,\pi$ [10-14], -0.7π [15] or $-3/4\,\pi$ [4, 16-21], and the optimum defocus for each is $\sqrt{4/3}\,[\mathrm{Sch}]$, $1.18[\mathrm{Sch}]$ or $\sqrt{3/2}\,[\mathrm{Sch}]$, respectively. Besides these different optimal defocus values have been proposed with τ in the range of approximately 2.5 to 3.1 (Table 1). These differences in the optimal defocus result in a difference of up to 1.13 times (0.71[Gl]/064[Gl]) in d_{Sch}.

The differences in Scherzer conditions and d_{Sch} that have been revealed as a result of the different views among researchers are somewhat acceptable from an academic point of view, but not from a practical one. The differences in Scherzer conditions and d_{Sch} are unfavorable to evaluating the instrumental performance of TEM manufacturers and users. When considering Scherzer conditions from the perspective of evaluating instrumental performance, it is important to consider the lens as an information transfer component.

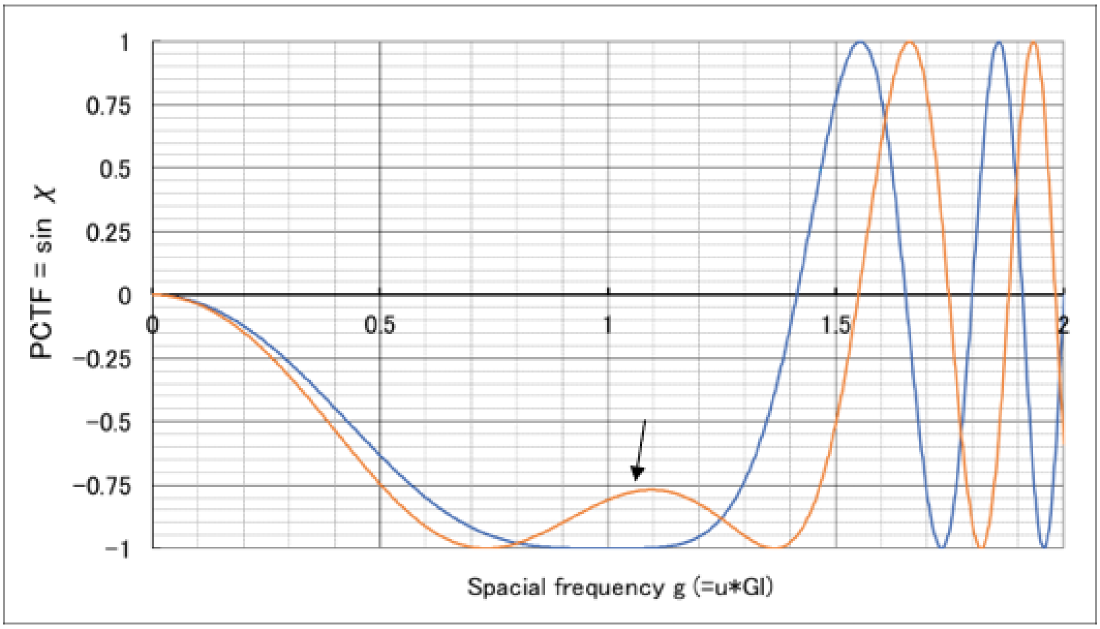

Figure 2. Phase Contrast Transfer Function for τ =2.5 (blue line) and 3.0 (orange line). The orange line shows a raised part (arrow) near the high-contrast area, but the high-contrast area is wider than the blue line.

d_{Sch} should be independent of the observer, and this paper presents the results of a study of d_{Sch} from the perspective of evaluating the performance of microstructure observation. Several different values of the Scherzer condition, which is the premise for defining d_{Sch}, have been employed [2, 4-34], as shown in Table 1. When d_{Sch} is calculated using these different coefficients, the TEM resolution is indeed non-uniform. This paper introduces the information transfer theory to overcome this circumstance and derives Scherzer conditions for evaluating instrument performance and the coefficients used in the equation defining Scherzer resolution. We thus propose an innovative method to estimate the defocus value from a series of through-focus images and then use the resulting real C_s to determine d_{Sch}.

τ	χ_{min}	$\sin(\chi_{min})$	Optimum focus; Δf [Sch]		Resolution: d_s [Gl], (1st zero position)		References
				Expressed in two decimal places		Expressed in two decimal places	
2.5066	$-\frac{1}{2}\pi$	-1.0000	1.0000	1.00	0.7071	0.71	[6], [7], [8], [9]
2.8025	-0.6250π	-0.9239	1.1180	1.12	0.6687		[22]
2.8100	-0.6277π	-0.9206	1.1204	1.12	0.6680	0.67	[this article]
2.8200	-0.6328π	-0.9142	1.1250	1.13	0.6667		[23]
2.8826	-0.6613π	-0.8744	1.1500	1.15	0.6594	0.66	[24]
2.8944	$-\frac{2}{3}\pi$	-0.8660	$\sqrt{4/3} = 1.1547$		0.6580		[10], [11], [12], [13], [14]
2.9659	-0.7000π	-0.8090	1.1832	1.18	0.6501		[15]
2.9765	-0.7050π	-0.7997	1.1874		0.6489		[5]
2.9829	-0.7081π	-0.7939	1.1900	1.19	0.6482		[25]
2.9841	-0.7086π	-0.7928	1.1905		0.6481	0.65	[26]
2.9870	-0.7100π	-0.7902	1.1916		0.6478		[27]
3.0000	-0.7162π	-0.7781	1.1968	1.20	0.6464		[2], [28]
3.0080	-0.7200π	-0.7705	1.2000		0.6455		[29], [30]
3.0581	-0.7442π	-0.7199	1.2094	1.21	0.6402		[31]
3.0315	-0.7313π	-0.7474	1.2200	1.22	0.6430		[32]
3.0700	$-\frac{3}{4}\pi$	-0.7071	$\sqrt{3/2} = 1.2247$		0.6389	0.64	[4], [16], [17], [18], [19] , [20], [21]
3.0765	-0.7532π	-0.7000	1.2273	1.23	0.6383		[33]
3.1207	-0.7750π	-0.6494	1.2450	1.25	0.6337		[34]

Table 1. Examples of various proposed Scherzer conditions.

2. Theoretical treatment of TEM resolution based on the information theory

Information theory [35, 36], established by C. E. Shannon in 1948, has allowed the mathematical treatment of information and communications and has developed into an academic field that is the foundation of today's digital society. According to the information theory, the amount of information ρ_H (bit/s) per 1 s of an analog signal $s(t)$ can be calculated from the minimum sampling rate at which the original signal $s(t)$ can be recovered without loss when $s(t)$ is discretized with time and amplitude. According to the sampling theorem, the sampling rate of time is twice the maximum frequency contained in $s(t)$. On the other hand, the sampling rate of amplitude (gradation) is determined by the S/N of the signal. And then ρ_H is given by Eq. (10),

$$\rho_H = \int_0^{W_f} \log_2 \left[\frac{|\tau(f)|^2 \cdot P_0 + N_P}{N_P}\right] df \tag{10}$$

where $\tau(f)$ is defined as the frequency characteristic of the signal $s(t)$ and P_0 and N_P are defined as the power (square of the amplitude) of the signal and the noise, respectively. Since the power is used in the calculation of the amount of information, $\tau(f)$ is squared and converted into the power in this equation. When $s(t)$ is replaced with the two-dimensional image signal $s_0(x, y)$, the amount of information (bit/nm^2) included in the image $s_0(x, y)$ can be calculated.

According to Sato's theory [37], the amount of information in SEM images is outlined. Fig. 3 shows the image formation model in SEM [37]. In this model, the SEM image is given by the sum of the convolution of the ideal sample image and the point spread function (PSF) representing the blurring of the optical system and the noise. Then the SEM image is obtained with variables in the reciprocal space, u_x and u_y, expressed as Eq. (11),

$$I_{SEM}(u_x, u_y) = S_0(u_x, u_y) \cdot \tau_{PSF}(u_x, u_y) + N(u_x, u_y) \tag{11}$$

where, $I_{SEM}(u_x, u_y)$, $S_0(u_x, u_y)$, $\tau_{PSF}(u_x, u_y)$, and $N(u_x, u_y)$ are Fourier transforms of the SEM image, the ideal sample image, the PSF, and the noise, respectively.

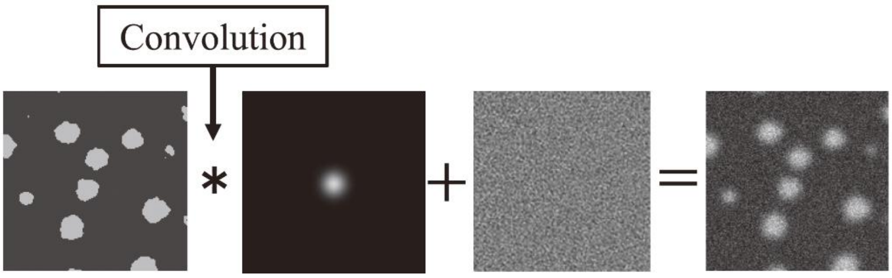

Fig. 3. Image formation model in SEM [45].

Assuming that P_0 is the statistical mean power of the ideal sample image $S_0(u_x, u_y)$ and $P_0/N_P = k_{SNR}^2$, Black and Linfoot [38] derived the amount of information H of the optical image as shown in Eq. (12), thereby making it possible to evaluate the optical system by the amount of information.

$$H = \pi D^2 \rho_H = \frac{\pi^2}{2} \int_0^2 \log_2 (1 + |\tau_{PSF}(\rho)|^2 \cdot k_{SNR}^2)\, \rho d\rho, \tag{12}$$

where D is the diffraction unit described as

$$D = \lambda/\alpha_{max} = 1/u_{max} = d_{min} \tag{13}$$

with the maximum diffraction angle, α_{max}, passing through the objective aperture, and u_{max} and d_{min}, the corresponding spatial frequency and the lattice spacing of the sample. $\boldsymbol{\rho}$ is a non-dimensional vector normalized by the radius of the pupil

$$\boldsymbol{\rho} = \boldsymbol{u}D = (\rho_x, \rho_y) \tag{14}$$

and ρ is a non-dimensional quantity in the radial direction

$$\rho = |\boldsymbol{\rho}|. \tag{15}$$

ρ_H is sometimes called the information passing capacity (IPC) of the optical system, and the amount of information H of the optical image can be interpreted as the IPC contained in a circle with the radius of D.

The optical transfer function (OTF, τ_{PSF}) is obtained by normalizing the point spread function at the origin and is calculated by the autocorrelation of the pupil function $G(\boldsymbol{u})$. Crewe and Salzman [39] obtained the OTF of the aberration-corrected STEM. By using the pupil function $G(\rho)$ of the SEM

$$G(\rho) = S_d(\rho)\exp\{i2\pi\phi(\rho)\} = S_d(\rho)\exp\{i(0.5\pi C_s\lambda^3u^4 - \pi\Delta f\lambda u^2)\} \tag{16-1}$$

and

$$S_d(\rho) = \begin{cases} 1\ at\ \rho \le 1 \\ 0\ at\ \rho > 1 \end{cases}, \tag{16-2}$$

Sato further derived the OTF $\tau_{PSF}(\rho)$ of the SEM affected by C_s and Δf analytically as [37, 40-42]

$$G(\rho) = S_d(\rho)\exp\{i2\pi\phi(\rho)\} = S_d(\rho)\exp\{i(0.5\pi C_s\lambda^3u^4 - \pi\Delta f\lambda u^2)\}\tau_{PSF}(\rho) = \frac{4}{\pi}\int_0^{1-\frac{\rho}{2}} W(\rho_x)d\rho_x, \tag{17}$$

where the integrand $W(\rho_x)$ is

$$W(\rho_x) = \frac{\cos(2\pi\phi_1(\rho_x))\cdot\mathcal{C}(\phi_2(\rho_x)) - \sin(2\pi\phi_1(\rho_x))\cdot\mathcal{S}(\phi_2(\rho_x))}{4\sqrt{B\rho\rho_x}}. \tag{18-1}$$

where

$$\mathcal{S}(x) = \int_0^x \sin\left(\frac{\pi}{2}t^2\right)dt \tag{18-2}$$

and

$$\mathcal{C}(x) = \int_0^x \cos\left(\frac{\pi}{2}t^2\right)dt \tag{18-3}$$

are Fresnel integrals, and ϕ_1 and ϕ_2 are expressed by Eqs. (19-1) and (19-2), respectively.

$$\phi_1(\rho_x) = \rho\rho_x(2A + B\rho^2 + 4B\rho_x^2) \tag{19-1}$$

$$\phi_2(\rho_x) = 4\sqrt{B\rho\rho_x\cdot\left(1 - \left(\rho_x + \frac{\rho}{2}\right)^2\right)} \tag{19-2}$$

Here, A and B are dimensionless quantities [39] expressed by Eqs. (20-1) and (20-2), and Δf and C_s are expressed by Eqs. (20-3) and (20-4), respectively.

$$A = -\frac{\Delta f\alpha_{max}}{2D} = -\frac{\Delta f\alpha_{max}^2}{2\lambda} \tag{20-1}$$

$$B = \frac{C_s \alpha_{max}^3}{4D} = \frac{C_s \alpha_{max}^4}{4\lambda} \quad (20\text{-}2)$$

$$\Delta f = -\frac{2\lambda}{\alpha_{max}^2} A \quad (20\text{-}3)$$

$$C_s = \frac{4\lambda}{\alpha_{max}^4} B \quad (20\text{-}4)$$

From these equations, it is understood that A and B are parameters that connect Δf and C_s with α_{max}. Since these equations hold for the optical transfer function (OTF, τ_{PSF}) of the TEM image as well according to the reciprocity theorem [43], the amount of information of the TEM image can be calculated by these equations.

When α_{max} is eliminated from the definition of A and B through Eqs. (20-1) and (20-2), respectively, Δf can be expressed using $(C_s\lambda)^{\frac{1}{2}}$ as a reference [3] as

$$\Delta f = -\frac{A}{\sqrt{B}} (C_s\lambda)^{\frac{1}{2}}. \quad (21)$$

From the above specifications, the position A where H becomes maximum for a certain B is considered the optimum and best focusing condition of TEM image observation. The relationship between A and B was thus obtained using numerical calculation.

We assumed $k_{SNR}^2 = 100$. Fig. 4 shows the coefficient $-A/\sqrt{B}$ of Eq. (21) for each value of B. It is understood that as B increases, $-A/\sqrt{B}$ converges to 1.12. Hence the best focus condition is

$$\Delta f = 1.12(C_s\lambda)^{\frac{1}{2}}. \quad (22)$$

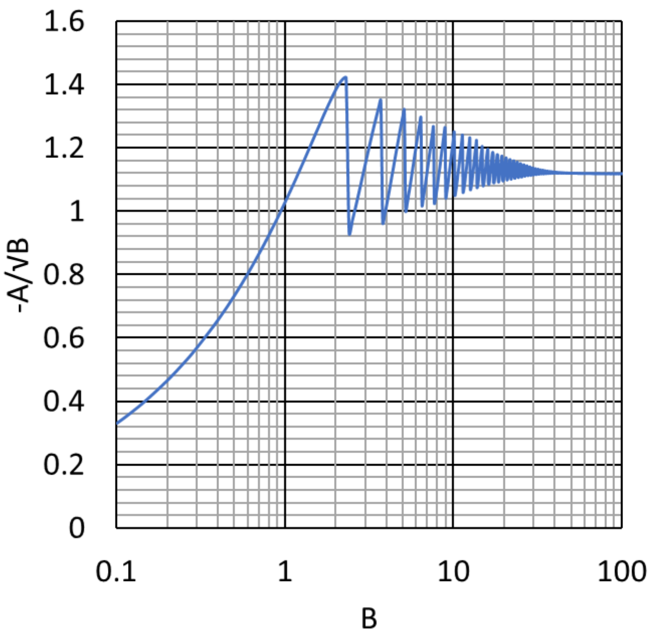

Fig. 4. Relationship between B and $-A/\sqrt{B}$.

and the best defocus value given by Eq. (22) is treated as Δf_{Sch}. Then, d_{Sch} is therefore given by Eq. (23).

$$d_{Sch} = 0.67(C_s\lambda^3)^{\frac{1}{4}} \quad (23)$$

3. Experimental procedure and measurement of point resolution

The point resolution of TEM can be determined by measuring the spatial frequency corresponding to the first dark ring appearing in the diffractogram obtained by the Fast Fourier Transform (FFT) of the image of an weak phase object recorded under Scherzer condition. In general, it is very difficult to acquire a single image satisfying Scherzer condition to determine the point resolution, so a through-focus series of TEM images should be acquired from front to back ranging across Scherzer focus.

(1) The initial step in the procedure is to determine the defocus value ($\Delta f_{n(k)}$) of the k^th image in the through-focusseries from the dark rings appearing in the diffractogram. Three dark rings (n=1~3) should be acquired for the measurement of the average defocus value ($\Delta f_{ave(k)}$).
(2) The real spherical aberration coefficient ($C_{s(r)}$) is determined using the variance (V) of Δf_n obtained from the three dark rings having a quadratic relationship against C_s.
(3) The real Scherzer focus value ($\Delta f_{Sch(r)}$) is calculated by applying $C_{s(r)}$ to Eq. (22).
(4) The point resolution is then determined using the linear relationship between Δf_{ave} and the square of the spatial frequency (u_1^2) corresponding to the first dark ring. The point resolution can therefore be determined by substituting $\Delta f_{Sch(r)}$ into a quasi-linear function from the graph of u_1^2 against Δf_{ave}.

Several papers have been reported on the measurement of the defocus value. For example, Thon used the "phase contrast transfer characteristic curve" to estimate the image defocus from the position of dark rings appearing in the diffractogram [44, 45]. Krivanek noted that the phase-distortion function expressed in Eq. (2) exhibits maximum phase contrast and zero contrast at odd and even multiples of π/2. Then he created a "diffractogram analysis graph", which is used to estimate the image defocus and spherical aberration coefficient [46]. A method proposed by Krivanek was extended further to develop a new defocus measurement method for images recorded for resolution measurement purposes, specifically.

When the defocus is in the range of about 10 to 15 nm above or below Scherzer focus, the relationship between the spatial frequency, u_n, corresponding to the n^th dark ring in the diffractogram and the phase-distortion function, $\chi(u_n)$, can be expressed as Eq. (24) and the defocus, Δf_n , can be calculated from the Eq. (25).

$$\chi(u_n) = \frac{\pi}{2} C_s \lambda^3 u_n^4 - \pi \Delta f_n \lambda u_n^2 = (n-1)\pi \qquad (n\text{: integer}) \tag{24}$$

$$\Delta f_n = \frac{1}{2} C_s \lambda^2 u_n^2 - \frac{n-1}{\lambda u_n^2} \tag{25}$$

A diffractogram of the k^th image of the through-focus series is shown in Fig. 5. As the field of view of the image with gold colloidal nanoparticles, the spatial frequency axis can be calibrated using the spots reflecting the lattice plane spacing of the gold appearing in the diffractogram. 1^st, 2^nd and 3^rd order dark rings are targeted for defocus measurement, and three defocus values, $\Delta f_{1(k)}$, $\Delta f_{2(k)}$ and $\Delta f_{3(k)}$, respectively, are obtained as measured results for a single image. If the C_s used in Eq. (25) is $C_{s(r)}$ exactly, then three defocus values should be the same value. In reality, variations due to measurement errors arise between them, thus the average value, $\Delta f_{ave(k)}$, of them is defined as the defocus of the k[th] image in Eq. (26).

$$\Delta f_{ave(k)} = \frac{1}{n}\sum_{n=1}^{3} \Delta f_{n(k)} \tag{26}$$

If given C_s deviate from $C_{s(r)}$, the difference between three defocus values also changes depending on the amount of deviation.

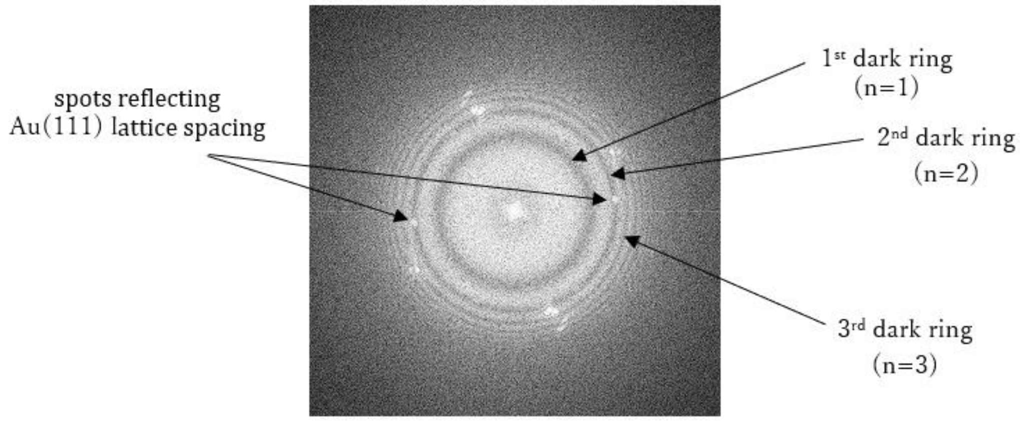

Fig. 5. Diffractogram of the kth image in the through-focus series.

$C_{s(r)}$ is then determined via the variance, $V_{(r)}$, of three defocus values, $\Delta f_{n(r)}$, obtained via a quadratic relationship with respect to C_s, and corresponding to the spatial frequencies ($u_{n(r)}$: $n = 1\sim3$), 1st zero to 3rd zero of the PCTF curve, can be expressed as in Eq. (27) with the average value ($\Delta f_{ave(r)}$) of three defocus values and $C_{s(r)}$.

$$V_{(r)} = \frac{1}{n}\sum_1^3\left(\Delta f_{n(r)} - \Delta f_{ave(r)}\right)^2 = \frac{1}{n}\sum_1^3\left(\left(\frac{1}{2}C_{s(r)}\lambda^2 u_n^2 - \frac{n-1}{\lambda u_n^2}\right) - \Delta f_{ave(r)}\right)^2 \tag{27}$$

When there is the slight deviation in the spherical aberration coefficient from $C_{s(r)}$, the deviated spherical aberration can be obtained by applying

$$C_{s(r+\delta)} = C_{s(r)} + \delta C_s \tag{28}$$

to formula (25) is defined as $\Delta f_{n(r+\delta)}$. The defocus shift (δf_n) between $\Delta f_{n(r+\delta)}$ and $\Delta f_{n(r)}$ can be expressed as Eq. (29), and the average defocus with deviation, $\Delta f_{ave(r+\delta)}$, and the variance with deviation, $V_{(r+\delta)}$, can also be expressed as Eqs. (30) and (31) respectively.

$$\delta f_n = 0.5\lambda^2(u_n)^2(\delta C_s) \tag{29}$$

$$\Delta f_{ave(r+\delta)} = \Delta f_{ave(r)} + \frac{1}{6}\lambda^2(\delta C_s)(u_1^2 + u_2^2 + u_3^2) \tag{30}$$

$$V_{(r+\delta)} = \frac{\lambda^4(\delta C_s)^2}{27}\left\{\left(u_1^2 - \frac{1}{2}u_2^2 - \frac{1}{2}u_3^2\right) + \left(u_2^2 - \frac{1}{2}u_3^2 - \frac{1}{2}u_1^2\right) + \left(u_3^2 - \frac{1}{2}u_1^2 - \frac{1}{2}u_2^2\right)\right\} \tag{31}$$

Eq. (29) suggests that $\Delta f_{1(r+\delta)} < \Delta f_{2(r+\delta)} < \Delta f_{3(r+\delta)}$ when δC_s is positive, and $\Delta f_{1(r+\delta)} > \Delta f_{2(r+\delta)} > \Delta f_{3(r+\delta)}$ when δC_s is negative. This characteristic can be used to determine whether the applied C_s has shifted in a positive or negative direction from the $C_{s(r)}$. In addition, Eq. (31) shows that $V_{(r+\delta)}$ is equal to the minimum value ($= 0$) when $\delta C_s = 0$ and increases quadratically with increasing δC_s.

In current TEMs, the provided C_s value, $C_{s(prvd)}$, by TEM manufacturers can be very close to the $C_{s(r)}$ value with slight deviation. Nonetheless, it is necessary to determine the $C_{s(r)}$ value as accurately as possible for the resolution measurements. Three C_s values, $C_{s(prvd)}$ and C_s values with±10% deviation from C_s, namely $0.9 \times C_{s(prvd)}$ and $1.1 \times C_{s(prvd)}$, are thus applied to Eq. (32) to obtain $V_{(r+\delta)}$ at each C_s value $V_{0.9\times C_{s(prvd)}}$, $V_{C_{s(prvd)}}$, $V_{1.1\times C_{s(prvd)}}$, respectively, and draw a graph of V against C_s as shown in Figure 6. As can be seen, the graph forms a quadratic function as shown in Eq. (32) with a, b and c as constants. Then, $C_{s(r)}$ value can be determined with the C_s value indicating the minimum value of V, V_{min}, it is expressed by Eq. (33).

$$V = \mathrm{a} \times (C_s)^2 + \mathrm{b} \times (C_s) + \mathrm{c} \tag{32}$$

$$C_{s(r)} = -\frac{\mathrm{b}}{2\mathrm{a}} \tag{33}$$

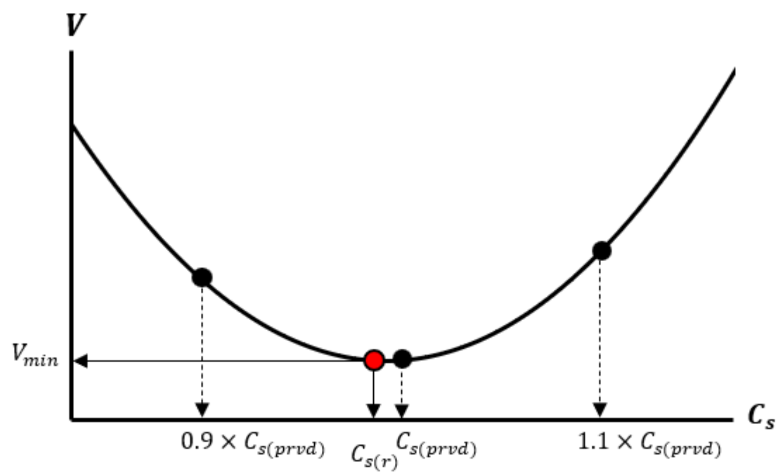

Fig. 6. Quadratic relationship between spherical aberration coefficient (C_s) and defocus variance (V). C_s value corresponding to minimum value of V, V_{min}, shows real spherical aberration coefficient, $C_{s(r)}$.

An example of a $C_{s(r)}$ measurement using a 200 kV FETEM with $C_{s(prvd)} = 1$ mm is described as follows. First, 29 through-focus images were captured. The defocus variance was then obtained for each of the 29 images with C_s values of 0.9 mm, 1 mm, or 1.1 mm. The relationship between the average of the 29 defocus variances and the C_s values are plotted as shown in Figure 7. The approximate quadratic function of the graph obtained using the Excel function was $V = 145.000 \times (C_s)^2 - 283.950 \times (C_s) + 139.611$. Finally, using Eq. (33), $C_{s(r)} = 0.979$ mm could be determined as the real spherical aberration coefficient.

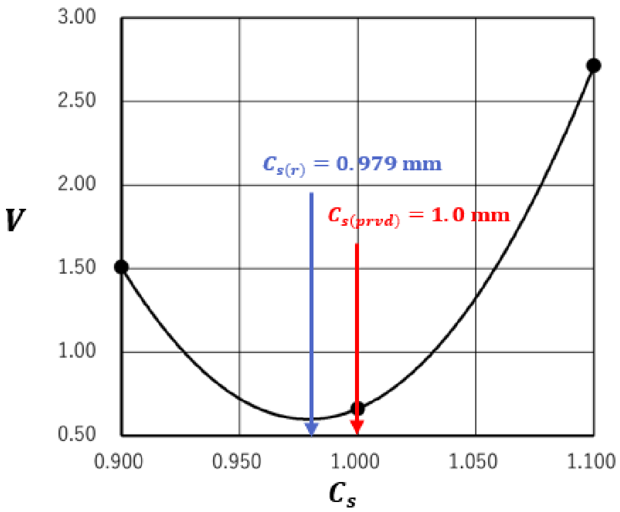

Fig. 7. Experimental results for determining the real spherical aberration coefficient ($C_{s(r)}$) using a 200 kV FETEM. The Cs value, which represents the minimum of the approximate quadratic function, indicates the $C_{s(r)}$. From the experimental results, $C_{s(r)}$ could be determined as 0.979 mm.

For a defocus close to Scherzer condition, $\chi(u_1) = 0$ is established for the spatial frequency (u_1) indicated by the first dark ring in the diffractogram. Therefore, from Eq. (24), it is clear that u_1^2 can be expressed as a linear function of Δf_1 as in Eq. (34).

$$u_1^2 = \frac{2}{C_s\lambda^2}\Delta f_1 \tag{34}$$

The resolution measurement procedure using the above relationship is described below. Apply determined $C_{s(r)} = 0.979$ mm to Eq. (25) to re-calculate $\Delta f_{ave(k)}$ and $u_{1(k)}^2$ for each of the 29 images of the through-focus series. The graph of $u_{1(k)}^2$ against $\Delta f_{ave(k)}$ was then plotted as shown in Figure 8 and an approximate linear function, as shown Eq. (35), was obtained using the Excel function.

$$u^2 = 0.325 \times (\Delta f) \tag{35}$$

Independently, Scherzer focus, $\Delta f_{Sch(r)}$, can be calculated from $C_{s(r)} = 0.979$ mm to Eq. (22) as 55.520 nm, resulting $4.248\ \mathrm{nm}^{-1}$ as the spatial frequency, $u_{Sch(r)}$. Scherzer resolution, $d_{Sch(r)}$, is then determined as 0.235 mm, which is in good agreement with optimal Scherzer resolution (=0.236 nm) calculated via Eq. (23) and proves that the instrument is performing as expected. In addition, the C_s value is calculated inversely from the coefficient (0.325) indicating that the slope of the linear function shown in Eq. (28) as 0.978 mm, which is also in good agreement with $C_{s(r)} =$ 0.979 mm, which confirms the precision of the current $C_{s(r)}$ measurement method.

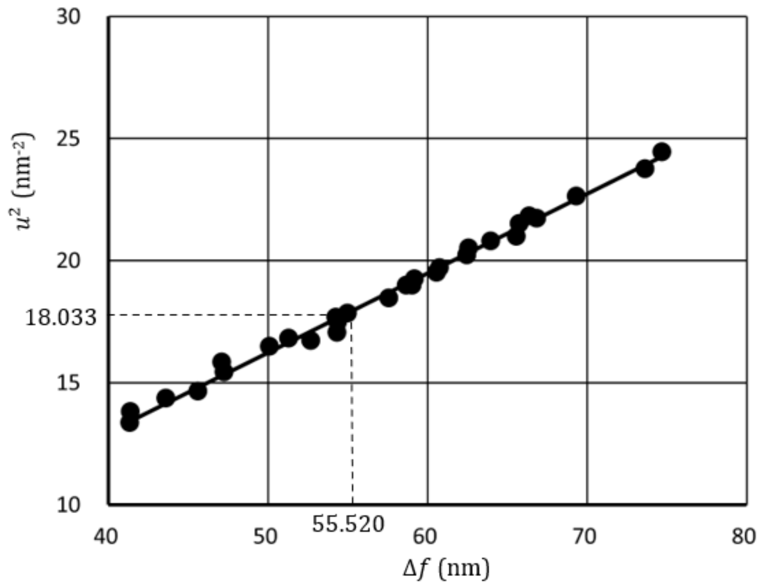

Fig. 8. Change in the square of the spatial frequency (u^2) corresponding to the first-order dark ring against defocus (Δf).

Graph shows the experimental results using a 200 kV FETEM (λ=0.00251 nm, $C_{s(r)}$ = 0.979 mm). Applying $\Delta f_{Scherzer(r)} = 55.520$ nm to the approximate linear function obtained from the graph, $d_{Scherzer(r)} = 0.235$ nm was determined as Scherzer resolution.

Conclusion

Acknowledgements

The authors express our thanks to Mr. K. Shiba and Dr. K. Kamei for providing us with the experimental data to analyze the Scherzer resolution. One of the authors (YT) would like to express his gratitude to Dr. M. Sato for the fruitful discussions in the calculation of the amount of information in TEM images.

References

[1] E. Ruska, M. Knoll; Z. techn. Physik., **12**, (1931), pp. 389-400, and 448, “Die magnetische Sammelspule für schnelle Elektronenstrahlen”

[2] O. Scherzer, J. Appl. Phys., **20**, (1949), pp.20-29, “The Theoretical Resolution Limit of the Electron Microscope“

[3] P. W. Hawkes; Ultramicrosc., 5, (1980), pp.67–70, “Units and conventions in electron microscopy, for use in ultramicroscopy”

[4] M. A. O'Keefe; Ultramicroscopy, **47**, (1992), pp.282-297, “”Resolution” in high-resolution electron microscopy“

[5] C. B. Eisenhandler and B. M. Siegel; Appl. Phys. Lett., 8, 10, (1966), pp.258-260, “A Zone-Plate Aperture for Enhancing Resolution in Phase-Contrast Electron

Microscopy”
[6] F. Zemlin, K. Weiss, P. Schiske, W. Kunath, K.H. Herrmann; Ultramicroscopy **3**, (1978), pp. 49-60, “Coma-free alignment of high resolution electron microscopes with the aid of optical diffractograms “
[7] W. O. Saxton; Computer techniques for image processing in electron microscopy. Advanced in Electronics and Electron Physics Supplement 10”, Academic Press, London, (1978)
[8] Helmut Kohl, and Ludwig Reimer; "Transmission Electron Microscopy. Physics of Image Formation, 5th Edition, Springer Series in Optical Sciences 36“, Springer Science+Business Media. LLC, (2008), p.3
[9] R. H. Wade and Joachim Frank; Optik, **49**, 1, (1977), pp.81-92, “Electron Microscope transfer functions for partially coherent axial illumination and chromatic defocus spread”
[10] John Maxwell Cowley; “Diffraction physics”, Elsevier, (1995), pp.296-299
[11] D. B. Williams and C. B. Carter; “Transmission electron microscopy: a textbook for materials science”, Springer Science & Business Media, (1996), pp.490-491
[12] Rafal E. Dunin-Borkowski and Lothar Houben; “Spherical and Chromatic Aberration Correction for Atomic-Resolution Liquid Cell Electron Microscopy, in Liquid Cell Electron Microscopy: 21”, Cambridge University Press, Ed. Frances M. Ross, (2016), pp.434-455
[13] Rolf Erni; “High-Resolution Transmission Electron Microscopy, An Introduction, in Aberration-corrected imaging in transmission electron microscopy, 2nd Edition”, World Scientific Publishing Company, (2015), pp.13-44
[14] M. Lentzen; Microsc. Microanal. 12, (2006), pp.191–205, “Progress in Aberration-Corrected High-Resolution Transmission Electron Microscopy Using Hardware Aberration Correction”
[15] S. Horiuchi; “Fundamentals of high-resolution transmission electron microscopy”, Elsevier Science & Technology, (1994), pp.148-166
[16] M. Lentzen; Microsc. Microanal., 14, (2008), pp.16–26, “Contrast Transfer and Resolution Limits for Sub-Angstrom High-Resolution Transmission Electron Microscopy”
[17] B. Fultz and J. M. Howe; Transmission Electron Microscopy and Diffractometry of Materials, 3rd Ed., Springer Berlin, Heidelberg, (2010)
[18] Jian Min Zuo and John C.H. Spence; Advanced Transmission Electron Microscopy - Imaging and Diffraction in Nanoscience, Springer Science+Business Media, New York, (2017)
[19] Earl J. Kirkland; Advanced Computing in Electron Microscopy, 3rd ed., Springer Nature, Switzerland AG, (2020)
[20] M. A. O’Keefe, C. J. D. Hetherington, Y. C. Wang, E. C. Nelson, J. H. Turner, C. Kisielowski, J. -O. Malm, R. Mueller, J. Ringnalda, M. Pan and A. Thust;

Ultramicroscopy, 89, (2001), pp.215–241, “Sub-Angstrom high-resolution transmission electron microscopy at 300 keV”

[21] John C.H. Spence; Experimental High Resolution Electron Microscopy, 2nd ed., Oxford University Press, New York, (1988)

[22] M. Sato; “Resolution, *in* Handbook of Charged Particle Optics 2nd Edition/ Edited by J. Orloff.“ CRC Press, (2009), PP.391-435

[23] Robert M. Glaeser; Journal of Microscopy, 117, 1, (1979), pp.77-91, "Prospects for extending the resolution limit of the electron microscope"

[24] S. J. Pennycook and P. D. Nellist; “Z-contrast Scanning Transmission Electron Microscopy, in Impact of Electron and Scanning Probe Microscopy on Materials Research, NATO Science series E”, Springer, Dordrecht, (1999), pp.161-207

[25] Helmut Kohl and Ludwig Reimer; "Transmission Electron Microscopy. Physics of Image Formation, 5th Edition, Springer Series in Optical Sciences 36“, Springer Science+Business Media. LLC, (2008), p.229

[26] K. J. Hanszen and Bodo Morgenstern; Zeitschrift für angewandte Physik, 19, 3, (1965), pp. 215-227, "Die Phasenkontrast-und Amplitudenkontrast-Übertragung des elektronenmikroskopischen Objektivs“

[27] C.B. Eisenhandler and B.M. Siegel; J. Appl. Phys., 37, (1966), pp.1613-1620, “Imaging of Single Atoms with the Electron Microscope by Phase Contrast”

[28] Akira Tonomura; "Electron holography." 2nd ed., Springer, Berlin, Heidelberg, (1999)

[29] M. Mitome, K. Takayanagi and Y. Tanishiro; Ultramicroscopy, 33, 4, (1990), pp.255-260, "Improvement of resolution by convergent-beam illumination in surface profile images of high resolution transmission electron microscopy"

[30] Miroslav Karlík; Materials Structure, 8, 1, (2001), pp.3-16, “Lattice Imaging in Transmission Electron Microscopy”

[31] R. Danev and K. Nagayama; Ultramicroscopy, 88, (2001), pp.243-252, “Transmission electron microscopy with Zernike phase plate”

[32] V. E. Cosslett; J. Microscopy, 128, (1982) pp.23-31, “Resolution and contrast in the electron microscope: an historical review”

[33] Peter W. Hawkes and John C. H. Spence, eds.; Science of microscopy. Vol. 1. New York: Springer, (2007)

[34] B. V. Johansen; Micron 4, 4, (1973), pp.446-472, "Bright field electron microscopy of biological specimens. I Obtaining the optimum contribution of phase contrast to image formation. “

[35] C. E. Shannon; The Bell system technical journal 27.3 (1948) 379-423, "A mathematical theory of communication".

[36] C. E. Shannon; The Bell system technical journal 27.3 (1948) 623-656, "A mathematical theory of communication".

[37] M. Sato; Kenbikyo 53 (2018) 127-133 (in Japanese), "Resolution theory for SEM

ans STEM".
[38] G. Black and E. H. Linfoot; Proc. R. Soc. Lond. A239 (1957) 522, “Spherical Aberration and the Information Content of Optical Images”.
[39] A. V. Crewe and D. B. Salzman; Ultramicroscopy 9 (1982) 373-378, “On the optimum resolution for a corrected STEM”.
[40] M. Sato and J. Orloff; Ultramicroscopy 41 (1992) 181-192, “A new concept of theoretical resolution of an optical system, comparison with experiment and optimum condition for a point source”.
[41] M. Sato, T. Ishitani, S. Watanabe and M. Nakagawa; Nucl. Instrum. Methods Phys. Res. A519 (2004) 280-285, “Evaluation of depth of field in SEM images in terms of the information-passing capacity (IPC) and contrast gradient in SEM image”.
[42] M. Sato; Resolution. Handbook of Charged Particle Optics Second Edition/Edited by J. Orloff. CRC Press, (2009) 391-435, “Resolution”.
[43] J. M. Cowley; Appl. Phys. Lett. 15 (1969) 58-59, “Image contrast in a transmission scanning electron microscope”.
[44] F. Thon; “Phase Contrast Electron Microscopy, in Electron Microscopy in Materials Science, Ed. U. Valdre”, Academic Press, New York and London, (1971), pp.570-625
[45] F. Thon; Z. Naturforsch., Vol. 21, (1966), pp.476-478, “Zur Defokussierungsab-hängigkeit des Phasenkontrastes bei der electronenmikrosckopischen Abbildung”
[46] O. L. Krivanek; Optik, 45, 1, (1976), pp.97-101, “A method for determining the coefficient of spherical aberration from a single electron micrograph”